PTEP

Prog. Theor. Exp. Phys. **2018**, 083B01 (20 pages)
DOI: 10.1093/ptep/pty080

Revisiting the A_4 model for leptons in light of NuFIT 3.2

Sin Kyu Kang[1,*], Yusuke Shimizu[2,*], Kenta Takagi[2,*], Shunya Takahashi[2], and Morimitsu Tanimoto[3]

[1] *School of Liberal Arts, Seoul-Tech, Seoul 139-743, Korea*
[2] *Graduate School of Science, Hiroshima University, Higashi-Hiroshima 739-8526, Japan*
[3] *Department of Physics, Niigata University, Niigata 950-2181, Japan*
*E-mail: skkang@seoultech.ac.kr, yu-shimizu@hiroshima-u.ac.jp, takagi-kenta@hiroshima-u.ac.jp

Received May 8, 2018; Revised June 15, 2018; Accepted June 21, 2018; Published August 14, 2018

We revisit the A_4 model for leptons in light of the new result of NuFIT 3.2. We introduce a new flavon η transforming as an A_4 singlet $1'$ or $1''$, which couples to both charged leptons and neutrinos in next-to-leading-order operators. The model consists of five parameters: the lightest neutrino mass m_1, the vacuum expectation value of η, and three CP-violating phases after inputting the experimental values of $\Delta m^2_{\rm atm}$ and $\Delta m^2_{\rm sol}$. The model with the $1''$ singlet flavon gives the prediction of $\sin^2\theta_{12}$ around the best fit of NuFIT 3.2 while staying near the maximal mixing of θ_{23}. Inputting the experimental mixing angles with the $1\,\sigma$ error-bar, the Dirac CP-violating phase is clearly predicted to be $|\delta_{\rm CP}| = 50$–$120°$, which will be tested by the precise observed value in the future. In order to get the best-fit value $\sin^2\theta_{23} = 0.538$, the sum of three neutrino masses is predicted to be larger than 90 meV. The cosmological observation for the sum of the neutrino masses will also provide a crucial test of our predictions. It is remarked that the model is consistent with the experimental data only for the normal hierarchy of neutrino masses.

Subject Index B40, B52, B54

1. Introduction

The origin of the quark/lepton flavor is still unknown in spite of the remarkable success of the standard model (SM). To reveal the underlying physics of flavors is challenging work. The recent developments in neutrino oscillation experiments have provided us with important clues to investigate flavor physics. Indeed, the neutrino oscillation experiments have determined precisely two neutrino mass-squared differences and three neutrino mixing angles. In particular, the recent data from both the T2K [1,2] and NOνA [3,4] experiments show us that the atmospheric neutrino mixing angle θ_{23} is favored near the maximal angle 45°. The global analysis by NuFIT 3.2 presents the best-fit $\theta_{23} = 47.2°$ for the normal hierarchy (NH) of neutrino masses [5]. The closer the observed θ_{23} is to the maximal mixing, the more likely we are to believe in some flavor symmetry behind it. In addition to the precise measurements of the mixing angles, the T2K and NOνA results strongly indicate the presence of CP violation in the neutrino oscillation [2,4]. Thus, we are in the era of the development of the flavor structure of the lepton mass matrices with a focus on the leptonic flavor mixing angles and CP-violating phase.

Before the reactor experiments measured a non-zero value for θ_{13} in 2012 [6,7], the paradigm of the tri–bimaximal (TBM) mixing [8,9], a highly symmetric mixing pattern for leptons, had attracted much attention. It is well known that this mixing pattern is derived in the framework of the A_4 flavor symmetry [10–13]. Therefore, non-Abelian discrete groups have become the center of attention in

Funded by SCOAP[3]

the flavor symmetry [14–17]. In order to obtain non-vanishing θ_{13}, two of the authors improved the A_4 model by a minimal modification by introducing another flavon that transforms as $1'('')$ of A_4 and couples only to the neutrino sector [18]. Then, the predicted values of θ_{13} are consistent with the experimental data. This pattern is essentially the trimaximal mixing TM_2 [19–21], which leads to $\sin^2\theta_{12} \geq 1/3$. However, the predicted $\sin^2\theta_{12}$ is outside the $2\,\sigma$ interval of the experimental data in the NuFIT 3.2 result [5]. Therefore, the A_4 model should be reconsidered in light of the implications of the new data from T2K and NOνA.

In this work, we introduce a new flavon transforming as an A_4 singlet, η ($1'$ or $1''$), which couples to both charged leptons and neutrinos in next-to-leading-order operators. The model consists of five parameters: the lightest neutrino mass m_1, the vacuum expectation value (VEV) of η, and three CP-violating phases after inputting the observed values of $\Delta m^2_{\mathrm{atm}}$ and $\Delta m^2_{\mathrm{sol}}$. The model with a $1''$ singlet flavon gives the prediction of $\sin^2\theta_{12}$ around the best fit of NuFIT 3.2 while staying near the maximal mixing of θ_{23}. The non-vanishing θ_{13} is derived from both charged lepton and neutrino sectors. Inputting the observed mixing angles with the $1\,\sigma$ error-bar, the CP-violating Dirac phase is clearly predicted to be $|\delta_{\mathrm{CP}}| = 50$–$120^\circ$. Therefore, the observation of the CP-violating phase is essential for testing the model in the future.

It is remarked that the model is consistent with the experimental data only for NH of neutrino masses. The inverted hierarchy (IH) of neutrino masses is not allowed in the recent experimental data. This situation comes from the singlet $1'$ or $1''$ flavon coupling to leptons in the next-to-leading order. It is in contrast with the model in Ref. [18] where both NH and IH are allowed.

We present our framework for the A_4 model in Sect. 2 where lepton mass matrices and VEVs of scalars are discussed. The numerical results are shown in Sect. 3. Section 4 is devoted to the summary. Appendix A shows the lepton mixing matrix and CP-violating measures that are used in this work. The relevant multiplication rules of A_4 are represented in Appendix B. The derivation of the lepton mixing matrix is given in Appendix C. Appendix D presents the distributions of our parameters that are used in our numerical calculations.

2. Our framework for the A_4 model

We discuss our A_4 model in the framework of supersymmetry (SUSY). In the non-Abelian finite group A_4, there are four irreducible representations: 1, $1'$, $1''$, and 3. The left-handed leptons l and right-handed charged leptons e^c, μ^c, τ^c are assigned to the triplet and singlets, respectively, as seen in Table 1. The two Higgs doublets (h_u, h_d) are assigned to the A_4 singlets, and their VEVs are denoted as (v_u, v_d) as usual. We introduce several flavons as listed in Table 1. The flavons ϕ_T and ϕ_S are A_4 triplets while ξ and $\tilde{\xi}$ are the same A_4 singlet 1. In addition, η and $\tilde{\eta}$ are the same non-trivial singlet $1''$ or $1'$. The A_4 flavor symmetry is spontaneously broken by VEVs of gauge singlet flavons, ϕ_T, ϕ_S, ξ, and η, whereas $\tilde{\xi}$ (1) and $\tilde{\eta}$ ($1''$, $1'$) are defined to have vanishing VEVs through the linear combinations of ξ and $\tilde{\xi}$ and η and $\tilde{\eta}$, respectively, as discussed in Ref. [13]. In the original model proposed by Altarelli and Feruglio [12,13], ϕ_T, ϕ_S, and ξ were introduced, and then the specific vacuum alignments of the triplet flavons led to the tri–bimaximal mixing where the lepton mixing angle θ_{13} vanishes. In 2011, two of the authors minimally modified the model by introducing an extra flavon η ($1'$) on top of those flavons to generate non-vanishing θ_{13} [18]. This modification of the model leads to the trimaximal mixing of neutrino flavors, so-called TM_2, which predicts $\sin^2\theta_{12} \geq 1/3$ [19–21]. Unfortunately, this prediction for θ_{12} is inconsistent with the data at the $2\,\sigma$ confidence level (C.L.) given in the NuFIT 3.2 result [5]. In this work, we force the flavon η ($1''$ or $1'$)

Table 1. Assignments of leptons, Higgs, flavons, and driving fields, where $\omega = \exp(2\pi i/3)$.

	l	e^c	μ^c	τ^c	$h_{u,d}$	ϕ_T	η	$\tilde{\eta}$	ϕ_S	ξ	$\tilde{\xi}$	Θ	ϕ_0^T	η_0	ϕ_0^S	ξ_0
$SU(2)$	2	1	1	1	2	1	1	1	1	1	1	1	1	1	1	1
A_4	$\mathbf{3}$	$\mathbf{1}$	$\mathbf{1}''$	$\mathbf{1}'$	$\mathbf{1}$	$\mathbf{3}$	$\mathbf{1}''(\mathbf{1}')$	$\mathbf{1}''(\mathbf{1}')$	$\mathbf{3}$	$\mathbf{1}$	$\mathbf{1}$	1	$\mathbf{3}$	$\mathbf{1}'(\mathbf{1}'')$	$\mathbf{3}$	$\mathbf{1}$
Z_3	ω	ω^2	ω^2	ω^2	1	1	1	1	ω	ω	ω	1	1	ω^2	ω	ω
$U(1)_{\mathrm{FN}}$	0	4	2	0	0	0	0	0	0	0	0	-1	0	0	0	0
$U(1)_R$	1	1	1	1	0	0	0	0	0	0	0	0	2	2	2	2

to couple to both the charged lepton and neutrino sectors in next-to-leading operators by assigning a Z_3 charge to η appropriately.

We impose the Z_3 symmetry to control Yukawa couplings in both the neutrino sector and charged lepton sector. The third row of Table 1 shows how each chiral multiplet transforms under Z_3 with its charge $\omega = \exp(2\pi i/3)$.

In order to obtain the natural hierarchy among lepton masses m_e, m_μ, and m_τ, we resort to the Froggatt–Nielsen mechanism [22] with an additional $U(1)_{\mathrm{FN}}$ symmetry under which only the right-handed lepton sector is charged. The field Θ denotes the Froggatt–Nielsen flavon in Table 1. The $U(1)_{\mathrm{FN}}$ charges are taken as (4, 2, 0) for (e^c, μ^c, τ^c), respectively. By assuming that Θ, carrying a negative unit charge of $U(1)_{\mathrm{FN}}$, acquires a VEV, the relevant mass ratio is reproduced through the Froggatt–Nielsen charges.

We also introduce a $U(1)_R$ symmetry in Table 1 to distinguish the flavons and driving fields ϕ_0^T, ϕ_0^S, ξ_0, and η_0, which are required to build a non-trivial scalar potential so as to realize the relevant symmetry breaking.

In this setup, the superpotential for respecting $A_4 \times Z_3 \times U(1)_{\mathrm{FN}} \times U(1)_R$ symmetry is written by introducing the cutoff scale Λ as

$$
\begin{aligned}
w &= w_Y + w_d, \\
w_Y &= w_l + w_\nu, \\
w_l &= y_e\, (\phi_T l)_{\mathbf{1}}\, e^c h_d \Theta^4/\Lambda^5 + y_\mu\, (\phi_T l)_{\mathbf{1}'}\, \mu^c h_d \Theta^2/\Lambda^3 + y_\tau\, (\phi_T l)_{\mathbf{1}''}\, \tau^c h_d/\Lambda \\
&\quad + y_e'\, (\phi_T l)_{\mathbf{1}'(\mathbf{1}'')}\, e^c h_d \eta \Theta^4/\Lambda^6 + y_\mu'\, (\phi_T l)_{\mathbf{1}''(\mathbf{1})}\, \mu^c h_d \eta \Theta^2/\Lambda^4 + y_\tau'\, (\phi_T l)_{\mathbf{1}(\mathbf{1}')}\, \tau^c h_d \eta/\Lambda^2, \\
w_\nu &= y_S (ll)_{\mathbf{3}} h_u h_u \phi_S/\Lambda^2 + y_\xi (ll)_{\mathbf{1}} h_u h_u \xi/\Lambda^2 \\
&\quad + y_1' (ll)_{\mathbf{1}} h_u h_u (\phi_S \phi_T)_{\mathbf{1}}/\Lambda^3 + y_2' (ll)_{\mathbf{1}'} h_u h_u (\phi_S \phi_T)_{\mathbf{1}''}/\Lambda^3 \\
&\quad + y_3' (ll)_{\mathbf{1}''} h_u h_u (\phi_S \phi_T)_{\mathbf{1}'}/\Lambda^3 + y_4' (ll)_{\mathbf{3}} h_u h_u (\phi_S \phi_T)_{\mathbf{3}}/\Lambda^3 \\
&\quad + y_5' (ll)_{\mathbf{3}} h_u h_u \phi_S \eta/\Lambda^3 + y_6' (ll)_{\mathbf{3}} h_u h_u \xi \phi_T/\Lambda^3 + y_7' (ll)_{\mathbf{1}'(\mathbf{1}'')} h_u h_u \xi \eta/\Lambda^3, \\
w_d &= w_d^T + w_d^S, \\
w_d^T &= -M \phi_0^T \phi_T + g \phi_0^T \phi_T \phi_T + \lambda \phi_0^T \phi_T \tilde{\eta} \\
&\quad - \lambda_1 \eta_0 \phi_T \phi_S + \lambda_2 \eta_0 \eta \xi + \lambda_3 \eta_0 \eta \tilde{\xi} + \lambda_4 \eta_0 \tilde{\eta} \xi + \lambda_5 \eta_0 \tilde{\eta} \tilde{\xi}, \\
w_d^S &= g_1 \phi_0^S \phi_S \phi_S + g_2 \phi_0^S \phi_S \tilde{\xi} - g_3 \xi_0 \phi_S \phi_S + g_4 \xi_0 \xi \xi + g_5 \xi_0 \xi \tilde{\xi} + g_6 \xi_0 \tilde{\xi} \tilde{\xi},
\end{aligned}
\tag{1}
$$

where the subscripts $1'(1'')$ in $(\phi_T l)_{\mathbf{1}'(\mathbf{1}'')}$, etc. correspond to the case of η for $1''(1')$. The Yukawa couplings y and y' are complex numbers of order one and M is a complex mass parameter, while g and

λ are trilinear couplings, which are also complex numbers of order one. Both leading operators and next-to-leading ones are included in w_Y, which leads to the flavor structure of lepton mass matrices including next-to-leading corrections.

On the other hand, w_d only contains leading operators, where we can force $\tilde{\xi}(\tilde{\eta})$ to couple with $\phi_0^S\phi_S$ ($\phi_0^T\phi_T$), but not $\xi(\eta)$ with it since $\tilde{\xi}$ and ξ($\tilde{\eta}$ and η) have the same quantum numbers [13]. We can study the vacuum structure and lepton mass matrices with these superpotentials.

2.1. *Vacuum alignments of flavons*

Let us investigate the vacuum alignments of flavons. The superpotentials w_d^T and w_d^S in Eq. (1) are written in terms of the components of triplet flavons:

$$
\begin{aligned}
w_d^T &= -M\left(\phi_{01}^T\phi_{T1}+\phi_{02}^T\phi_{T3}+\phi_{03}^T\phi_{T2}\right)+\lambda\left(\phi_{01}^T\phi_{T2}+\phi_{02}^T\phi_{T1}+\phi_{03}^T\phi_{T3}\right)\tilde{\eta}\\
&\quad+\frac{2g}{3}\left[\phi_{01}^T\left(\phi_{T1}^2-\phi_{T2}\phi_{T3}\right)+\phi_{02}^T\left(\phi_{T2}^2-\phi_{T1}\phi_{T3}\right)+\phi_{03}^T\left(\phi_{T3}^2-\phi_{T1}\phi_{T2}\right)\right]\\
&\quad-\lambda_1\eta_0\left(\phi_{T2}\phi_{S2}+\phi_{T1}\phi_{S3}+\phi_{T3}\phi_{S1}\right)+\lambda_2\eta_0\eta\xi+\lambda_3\eta_0\eta\tilde{\xi}+\lambda_4\eta_0\tilde{\eta}\xi+\lambda_5\eta_0\tilde{\eta}\tilde{\xi},\\
w_d^S &= \frac{2g_1}{3}\left[\phi_{01}^S\left(\phi_{S1}^2-\phi_{S2}\phi_{S3}\right)+\phi_{02}^S\left(\phi_{S2}^2-\phi_{S1}\phi_{S3}\right)+\phi_{03}^S\left(\phi_{S3}^2-\phi_{S1}\phi_{S2}\right)\right]\\
&\quad+g_2\left(\phi_{01}^S\phi_{S1}+\phi_{02}^S\phi_{S3}+\phi_{03}^S\phi_{S2}\right)\tilde{\xi}\\
&\quad-g_3\xi_0\left(\phi_{S1}^2+2\phi_{S2}\phi_{S3}\right)+g_4\xi_0\xi^2+g_5\xi_0\xi\tilde{\xi}+g_6\xi_0\tilde{\xi}^2,
\end{aligned}
\tag{2}
$$

where w_d^S is the same superpotential given in Ref. [13]. Note that new terms including η and $\tilde{\eta}$ are added in w_d^T.

Then, the scalar potential of the F-term is given as

$$
\begin{aligned}
V &\equiv V_T+V_S,\\
V_T &= \sum_i\left|\frac{\partial w_d^T}{\partial\phi_{0i}^T}\right|^2+\text{h.c.}\\
&= 2\left|-M\phi_{T1}+\lambda\phi_{T2}\tilde{\eta}+\frac{2g}{3}\left(\phi_{T1}^2-\phi_{T2}\phi_{T3}\right)\right|^2\\
&\quad+2\left|-M\phi_{T3}+\lambda\phi_{T1}\tilde{\eta}+\frac{2g}{3}\left(\phi_{T2}^2-\phi_{T1}\phi_{T3}\right)\right|^2\\
&\quad+2\left|-M\phi_{T2}+\lambda\phi_{T3}\tilde{\eta}+\frac{2g}{3}\left(\phi_{T3}^2-\phi_{T1}\phi_{T2}\right)\right|^2\\
&\quad+2\left|-\lambda_1\left(\phi_{T2}\phi_{S2}+\phi_{T1}\phi_{S3}+\phi_{T3}\phi_{S1}\right)+\lambda_2\eta\xi+\lambda_3\eta\tilde{\xi}+\lambda_4\tilde{\eta}\xi+\lambda_5\tilde{\eta}\tilde{\xi}\right|^2,\\
V_S &= \sum\left|\frac{\partial w_d^S}{\partial X}\right|^2+\text{h.c.}\\
&= 2\left|\frac{2g_1}{3}\left(\phi_{S1}^2-\phi_{S2}\phi_{S3}\right)+g_2\phi_{S1}\tilde{\xi}\right|^2+2\left|\frac{2g_1}{3}\left(\phi_{S2}^2-\phi_{S1}\phi_{S3}\right)+g_2\phi_{S3}\tilde{\xi}\right|^2
\end{aligned}
$$

$$+ 2\left|\frac{2g_1}{3}\left(\phi_{S3}^2-\phi_{S1}\phi_{S2}\right)+g_2\phi_{S2}\tilde{\xi}\right|^2$$
$$+ 2\left|-g_3\left(\phi_{S1}^2+2\phi_{S2}\phi_{S3}\right)+g_4\xi^2+g_5\xi\tilde{\xi}+g_6\tilde{\xi}^2\right|^2. \tag{3}$$

The vacuum alignments of ϕ_T, ϕ_S and VEVs of η, $\tilde{\eta}$, ξ, and $\tilde{\xi}$ are derived from the condition of the potential minimum, i.e., $V_T = 0$ and $V_S = 0$ in Eq. (3), as

$$\langle\phi_T\rangle = v_T(1,0,0), \quad \langle\phi_S\rangle = v_S(1,1,1), \quad \langle\eta\rangle = q, \quad \langle\tilde{\eta}\rangle = 0, \quad \langle\xi\rangle = u, \quad \langle\tilde{\xi}\rangle = 0,$$
$$v_T = \frac{3M}{2g}, \qquad v_S^2 = \frac{g_4}{3g_3}u^2, \qquad q = \frac{\lambda_1 v_T v_S}{\lambda_2 u} = \frac{\lambda_1}{\lambda_2}\sqrt{\frac{g_4}{3g_3}}v_T, \tag{4}$$

where the VEVs of $\tilde{\xi}$ and $\tilde{\eta}$ are taken to be zero by the linear transformation of ξ and $\tilde{\xi}$ (η and $\tilde{\eta}$) without loss of generality. The coefficients λ_i and g_i are of order one since these flavons have no FN charges. Therefore, the VEVs of η and ξ are of the same order as v_T and v_S, respectively. In our numerical analyses, q/Λ is scanned around v_T/Λ, which is fixed by the tau-lepton mass.

On the other hand, the FN flavon Θ is not contained in w_d due to the $U(1)_{\mathrm{FN}}$ invariance. The VEV of Θ can be derived from the scalar potential of the D-term by assuming gauged $U(1)_{\mathrm{FN}}$. The Fayet–Iliopolos term leads to the non-vanishing VEV of Θ as discussed in Ref. [23]. Thus, its VEV is determined independently of v_T, v_S, u, and q.

2.2. Lepton mass matrices

The explicit lepton mass matrices are derived from the superpotentials w_l and w_ν in Eq. (1) by use of the multiplication rule of A_4 given in Appendix B. Let us begin with writing down the charged lepton mass matrices by imposing the vacuum alignments in Eq. (4) as:

$$M_\ell = v_d\alpha_\ell\begin{pmatrix} y_e\lambda^4 & 0 & y'_\tau\alpha_\eta \\ y'_e\alpha_\eta\lambda^4 & y_\mu\lambda^2 & 0 \\ 0 & y'_\mu\alpha_\eta\lambda^2 & y_\tau \end{pmatrix} \text{ for } \eta(1''), \quad v_d\alpha_\ell\begin{pmatrix} y_e\lambda^4 & y'_\mu\alpha_\eta\lambda^2 & 0 \\ 0 & y_\mu\lambda^2 & y'_\tau\alpha_\eta \\ y'_e\alpha_\eta\lambda^4 & 0 & y_\tau \end{pmatrix} \text{ for } \eta(1'), \tag{5}$$

where α_ℓ, α_η, and λ are defined in terms of the VEVs of ϕ_T, η, and Θ, respectively:

$$\alpha_\ell \equiv \frac{\langle\phi_T\rangle}{\Lambda} = \frac{v_T}{\Lambda}, \qquad \alpha_\eta \equiv \frac{\langle\eta\rangle}{\Lambda} = \frac{q}{\Lambda}, \qquad \lambda \equiv \frac{\langle\Theta\rangle}{\Lambda}. \tag{6}$$

We note that the off-diagonal elements arise from the next-to-leading operators.

The left-handed mixing matrix of the charged lepton is derived by diagonalizing $M_\ell M_\ell^\dagger$. We obtain the mixing matrix $U_\ell^\dagger$ approximately for the cases of η being $1''$ or $1'$ of A_4 as (more explicitly presented in Appendix C):

$$U_\ell^\dagger \simeq \frac{1}{\sqrt{1+\alpha_\eta^{\tau 2}}}\begin{pmatrix} 1 & -\mathcal{O}(\alpha_\eta^2) & \alpha_\eta^\tau e^{i\varphi} \\ \mathcal{O}(\alpha_\eta^2) & \sqrt{1+\alpha_\eta^{\tau 2}} & \mathcal{O}(\alpha_\eta\lambda^4) \\ -\alpha_\eta^\tau e^{-i\varphi} & \mathcal{O}(\alpha_\eta^3) & 1 \end{pmatrix} \quad \text{for } \eta(1''),$$

$$U_\ell^\dagger \simeq \frac{1}{\sqrt{1+\alpha_\eta^{\mu 2}}}\frac{1}{\sqrt{1+\alpha_\eta^{\tau 2}}}\begin{pmatrix} \sqrt{1+\alpha_\eta^{\tau 2}} & \sqrt{1+\alpha_\eta^{\tau 2}}\,\alpha_\eta^\mu e^{i\varphi'} & \mathcal{O}(\alpha_\eta^2\lambda^4) \\ -\alpha_\eta^\mu e^{-i\varphi'} & 1 & \dfrac{\sqrt{1+\alpha_\eta^{\mu 2}}\,\alpha_\eta^\tau e^{i\varphi}}{\sqrt{1+\alpha_\eta^{\mu 2}}} \\ \mathcal{O}(\alpha_\eta^2) & -\alpha_\eta^\tau e^{-i\varphi} & \end{pmatrix} \quad \text{for } \eta(1'), \tag{7}$$

where

$$\alpha_\eta^\tau e^{i\varphi} \equiv \frac{y'_\tau}{y_\tau}\alpha_\eta, \qquad \alpha_\eta^\mu e^{i\varphi'} \equiv \frac{y'_\mu}{y_\mu}\alpha_\eta. \tag{8}$$

The mass eigenvalues m_e^2, m_μ^2, and m_τ^2 are obtained by $U_\ell M_\ell M_\ell^\dagger U_\ell^\dagger$ as shown in Appendix C.

In the leading-order approximation, U_ℓ depends on one real parameter α_η^τ and one phase φ for the case of $\eta(1'')$, whereas it depends on α_η^τ, α_η^μ, φ, and φ' for the case of $\eta(1')$. The parameter α_η is expected to be much less than 1 as discussed in the next section. As seen in Eq. (7), the off-diagonal (1,3) and (3,1) entries in $U_\ell^\dagger$ are dominant for the case of $\eta(1'')$ while the off-diagonal (1,2) and (2,3) (also (2.1) and (3,2)) entries in $U_\ell^\dagger$ are dominant for the case of $\eta(1')$. Thus, it is expected that the assignments of $\eta(1'')$ and $\eta(1')$ give rise to different predictions of the mixing and the CP violation. It is found that the effects of the next-to-leading terms of $\mathcal{O}(\alpha_\eta^2)$, $\mathcal{O}(\alpha_\eta^3)$, and $\mathcal{O}(\alpha_\eta\lambda^4)$ in the mixing matrix $U_\ell^\dagger$ are negligibly small by our numerical estimation.

The neutrino mass matrix is derived from the superpotential w_ν in Eq. (1) by imposing the vacuum alignments given in Eq. (4). The next-to-leading operator $y'_5 llh_u h_u \phi_S \eta$ can be absorbed in the leading one $y_S llh_u h_u \phi_S$ due to the alignment of $\langle\phi_S\rangle \propto (1,1,1)$. Although the next-to-leading operators $llh_u h_u \phi_S \phi_T$ and $llh_u h_u \phi_T \xi$ cannot be absorbed in the leading one, their effects are expected to be suppressed because $\langle\phi_T\rangle/\Lambda$ is fixed to be small. We have confirmed that the effect of these next-to-leading operators is negligibly small in our numerical calculations.

On the other hand, the operator $y'_7 llh_u h_u \xi\eta$ leads to a significant contribution to the neutrino mass matrix because $\langle\eta\rangle/\Lambda$ could be significantly larger than $\langle\phi_T\rangle/\Lambda$ as discussed in Appendix D. For $\eta(1'')$, we have

$$M_\nu = a\begin{pmatrix}1&0&0\\0&1&0\\0&0&1\end{pmatrix} + b\begin{pmatrix}1&1&1\\1&1&1\\1&1&1\end{pmatrix} + c\begin{pmatrix}1&0&0\\0&0&1\\0&1&0\end{pmatrix} + d\begin{pmatrix}0&1&0\\1&0&0\\0&0&1\end{pmatrix}, \tag{9}$$

where the coefficients a, b, c, and d are given in terms of the Yukawa couplings and VEVs of flavons as follows:

$$a = \frac{y_S\alpha_\nu}{\Lambda}v_u^2, \quad b = -\frac{y_S\alpha_\nu}{3\Lambda}v_u^2, \quad c = \frac{y_\xi\alpha_\xi}{\Lambda}v_u^2, \quad d = \frac{y'_7\alpha_\xi\alpha_\eta}{\Lambda}v_u^2, \tag{10}$$

with

$$\alpha_\nu \equiv \frac{\langle\phi_S\rangle}{\Lambda} = \frac{v_S}{\Lambda}, \qquad \alpha_\xi \equiv \frac{\langle\xi\rangle}{\Lambda} = \frac{u}{\Lambda}\ . \tag{11}$$

Since the parameter d is induced from the next-to-leading operator $ll\xi\eta h_u h_u$, the magnitude of d is expected to be much smaller than a, b, and c.

For $\eta(1')$, we get

$$M_\nu = a\begin{pmatrix}1&0&0\\0&1&0\\0&0&1\end{pmatrix} + b\begin{pmatrix}1&1&1\\1&1&1\\1&1&1\end{pmatrix} + c\begin{pmatrix}1&0&0\\0&0&1\\0&1&0\end{pmatrix} + d\begin{pmatrix}0&0&1\\0&1&0\\1&0&0\end{pmatrix}, \tag{12}$$

where the last matrix of the right-hand side is a different one compared with the case of $\eta(1'')$.

There are three complex parameters in the model since the coefficient b is given in terms of a $(a+3b=0)$. We take a to be real without loss of generality and reparametrize them as follows:

$$a \to a, \quad c \to c\, e^{i\phi_c}, \quad d \to d\, e^{i\phi_d}, \tag{13}$$

where a, c, and d are real parameters and ϕ_c, ϕ_d are CP-violating phases.

For the lepton mixing matrix, Harrison–Perkins–Scott proposed a simple form of the mixing matrix, so-called TBM mixing [8,9],

$$V_{\text{TBM}} = \begin{pmatrix} \frac{2}{\sqrt{6}} & \frac{1}{\sqrt{3}} & 0 \\ -\frac{1}{\sqrt{6}} & \frac{1}{\sqrt{3}} & -\frac{1}{\sqrt{2}} \\ -\frac{1}{\sqrt{6}} & \frac{1}{\sqrt{3}} & \frac{1}{\sqrt{2}} \end{pmatrix}, \tag{14}$$

by which M_ν is diagonalized in the case of $d=0$. We obtain the neutrino mass matrix in the TBM basis by rotating it with V_{TBM} as:

$$\hat{M}_\nu = V_{\text{TBM}}^T M_\nu V_{\text{TBM}} = \begin{pmatrix} a + ce^{i\phi_c} - \frac{d}{2}e^{i\phi_d} & 0 & \mp\frac{\sqrt{3}}{2}de^{i\phi_d} \\ 0 & ce^{i\phi_c} + de^{i\phi_d} & 0 \\ \mp\frac{\sqrt{3}}{2}de^{i\phi_d} & 0 & a - ce^{i\phi_c} + \frac{d}{2}e^{i\phi_d} \end{pmatrix}, \tag{15}$$

where the upper (lower) sign in front of the (1,3) and (3,1) components corresponds to η transforming as $1''(1')$. The neutrino mass eigenvalues are explicitly given in Appendix C.

The mixing matrix U_ν is derived from the diagonalization of $\hat{M}_\nu \hat{M}_\nu^\dagger$ apart from the Majorana phases such as

$$U_\nu\ (\hat{M}_\nu \hat{M}_\nu^\dagger)\ U_\nu^\dagger = \begin{pmatrix} m_1^2 & 0 & 0 \\ 0 & m_2^2 & 0 \\ 0 & 0 & m_3^2 \end{pmatrix}. \tag{16}$$

As shown in Appendix C, we get

$$U_\nu^\dagger = \begin{pmatrix} \cos\theta & 0 & \sin\theta e^{-i\sigma} \\ 0 & 1 & 0 \\ -\sin\theta e^{i\sigma} & 0 & \cos\theta \end{pmatrix}, \tag{17}$$

where θ and σ are given in terms of parameters in the neutrino mass matrix.

As seen in Eq. (10), the parameter d is related to c as

$$\frac{d}{c} = \left|\frac{y_7'}{y_\xi}\right| \alpha_\eta \equiv \alpha_\eta^\nu, \tag{18}$$

where y_7' and y_ξ are coefficients of order one. On the other hand, a and c are given in terms of m_1, α_η^ν, and the experimental data Δm^2_{sol} and Δm^2_{atm} as shown in Appendix C. Therefore, m_1 and α_η^ν are free parameters in addition to ϕ_c and ϕ_d in our model.

It is remarkable that neutrino mass eigenvalues do not satisfy $\Delta m^2_{\text{sol}} > 0$ for the case of IH of neutrino masses as discussed in Appendix C because of the relations $a \sim c$ and $c \gg d$ in our model. This is understandable by considering the case of the $d=0$ limit, which corresponds to the exact TBM mixing. It is allowed only for NH of the neutrino mass spectrum.

Finally, the Pontecorvo–Maki–Nakagawa–Sakata (PMNS) matrix [24,25] is given as

$$U_{\rm PMNS} = U_\ell \, V_{\rm TBM} \, U_\nu^\dagger \, P, \tag{19}$$

where P is the diagonal matrix responsible for the Majorana phases obtained from

$$PU_\nu \hat{M}_\nu U_\nu^T P = {\rm diag}\{m_1, m_2, m_3\}, \tag{20}$$

where m_1, m_2, and m_3 are real positive neutrino masses.

The effective mass for the neutrinoless double beta ($0\nu\beta\beta$) decay is given as follows:

$$|m_{ee}| = \left| m_1 U_{e1}^2 + m_2 U_{e2}^2 + m_3 U_{e3}^2 \right|, \tag{21}$$

where U_{ei} denotes each component of the PMNS matrix $U_{\rm PMNS}$, which includes the Majorana phases.

From Eq. (19), we can write down the three neutrino mixing angles of Appendix A in terms of our model parameters for the case of the $1''$ singlet η, which shows how experimental results can be accommodated in our model:

$$\begin{aligned} \sin\theta_{12} &\simeq \frac{1}{\sqrt{1+\alpha_\eta^{\tau 2}}} \frac{1}{\sqrt{3}} \left| 1 - \alpha_\eta^\tau e^{i\varphi} \right|, \\ \sin\theta_{13} &\simeq \frac{1}{\sqrt{1+\alpha_\eta^{\tau 2}}} \left| \frac{2}{\sqrt{6}} \sin\theta e^{-i\sigma} - \frac{1}{\sqrt{2}} \alpha_\eta^\tau \cos\theta e^{i\varphi} \right|, \\ \sin\theta_{23} &\simeq \left| -\frac{1}{\sqrt{2}} \cos\theta - \frac{1}{\sqrt{6}} \sin\theta e^{-i\sigma} \right|, \end{aligned} \tag{22}$$

where the next-to-leading terms are omitted. It is remarkable that $\sin\theta_{13}$ is composed of contributions from both the charged leptons and neutrinos. On the other hand, the deviation from the trimaximal mixing of θ_{12} comes from the charged lepton sector, whereas the deviation from the maximal mixing of θ_{23} comes from the neutrino sector. Since these are given in terms of four independent parameters, we cannot obtain the sum rules in the PMNS matrix elements. However, the tau-lepton mass helps us to predict the allowed region of the CP-violating Dirac phase $\delta_{\rm CP}$ and Majorana phases α_{21} and α_{31} as discussed in the next section.

3. Numerical results

First, we present the framework of our calculations to predict the CP-violating Dirac phase $\delta_{\rm CP}$ and Majorana phases α_{21} and α_{31}. We explain how to get our predictions in terms of three real parameters α_η^τ, α_η^ν, and m_1 on top of three phases φ, ϕ_c, and ϕ_d for NH of neutrino masses. We can put for simplicity

$$\alpha_\eta = \alpha_\eta^\tau = \alpha_\eta^\nu, \tag{23}$$

i.e., $|y_7'/y_\xi| = |y_\tau'/y_\tau| = 1$ since all Yukawa couplings are of order one.

The result of NuFIT 3.2 [5] is used as the input data to constrain the unknown parameters. By taking $m_3^2 - m_1^2 = \Delta m_{\rm atm}^2$ and $m_2^2 - m_1^2 = \Delta m_{\rm sol}^2$ with the $3\,\sigma$ and $1\,\sigma$ data given in Table 2, a, c, and d are fixed in terms of m_1, α_η, ϕ_c, and ϕ_d. There is also the CP-violating phase φ in the charged lepton mixing matrix. In our numerical analysis, we perform a parameter scan over these three phases and m_1 by generating random numbers. The scan ranges of the parameters are $-\pi \lesssim (\varphi, \phi_c, \phi_d) \lesssim \pi$ and

Table 2. The best-fit, 1σ, and 3σ ranges of neutrino oscillation parameters from NuFIT 3.2 for NH [5].

Observable	Best fit and 1σ	3σ range
$\Delta m^2_{\rm atm}$	$(2.494^{+0.033}_{-0.031}) \times 10^{-3}\,{\rm eV}^2$	$(2.399\text{–}2.593) \times 10^{-3}\,{\rm eV}^2$
$\Delta m^2_{\rm sol}$	$(7.40^{+0.21}_{-0.20}) \times 10^{-5}\,{\rm eV}^2$	$(6.80\text{–}8.02) \times 10^{-5}\,{\rm eV}^2$
$\sin^2\theta_{23}$	$0.538^{+0.033}_{-0.069}$	0.418–0.613
$\sin^2\theta_{12}$	$0.307^{+0.013}_{-0.012}$	0.272–0.346
$\sin^2\theta_{13}$	$0.022\,06^{+0.000\,75}_{-0.000\,75}$	0.019 81–0.024 36

$0 \lesssim m_1 \lesssim 50$ meV. Note that the range of m_1 is restricted by the lower bound of the cosmological data for the sum of the neutrino masses, 160 meV [26]. The parameter α_η is constrained by the tau-lepton mass:

$$m_\tau = |y_\tau|\alpha_\ell v_d, \tag{24}$$

which gives $\alpha_\ell = 0.0316$ and 0.010 for the minimal supersymmetric standard model (MSSM) with $\tan\beta = 3$ and SM, respectively. Here we put $|y_\tau| = 1$. Since α_η is of the same order as α_ℓ as seen in Eq. (4), we vary the parameter α_η around $\alpha_\ell = 0.0316$ (0.010) by using the Γ distribution (χ^2 distribution), which is presented in Appendix D.

We calculate three neutrino mixing angles in terms of the model parameters while keeping the parameter sets leading to values allowed by the experimental data at 1σ and 3σ C.L. as given in Table 2. Then, we calculate the CP-violating phases and $|m_{ee}|$ with those selected parameter sets. Accumulating enough parameter sets surviving the above procedure, we make various scatter plots to show how the observables depend on the model parameters.

In Sect. 3.1, we show our numerical results for $\eta(1'')$. The numerical results for $\eta(1')$ are briefly shown in Sect. 3.2.

3.1. *Case of a* $1''$ *singlet* η

Let us show numerical results for the case of a $1''$ singlet η. We analyze only the case of NH of neutrino masses since the case of IH of neutrino masses is inconsistent with the experimental data as discussed in Appendix C.

First, we show the prediction of δ_{CP} versus $\sin^2\theta_{23}$ in Fig. 1 where the blue and green dots correspond to the input of the 3σ and 1σ data in Table 2, respectively. This result is similar to the prediction of TM_2 since the deviation from the maximal mixing of θ_{23} is due to the extra (1,3) family rotation of the neutrino mass matrix in Eq. (15). In order to compare our prediction with the TM_2 result [27,28], we show its prediction by a red curve, which is obtained by taking the best-fit data in Table 2. We see that our predicted region is inside the TM_2 boundary. For the maximal mixing $\theta_{23} = \pi/4$, the absolute value of δ_{CP} is expected to be 60–90°. It is also predicted to be $90° \lesssim |\delta_{CP}| \lesssim 110°$ at the best fit of $\sin^2\theta_{23} = 0.538$. All values between $-180°$ and $180°$ are allowed for δ_{CP} in the case of the input data at 3σ as seen in Fig. 1. However, for the input data at 1σ, $|\delta_{CP}|$ is restricted to 50–120°, which is completely consistent with the present data at 1σ, $-157° \lesssim \delta_{CP} \lesssim -83°$, apart from its sign. Thus, the precise data of θ_{23} and δ_{CP} would provide us with a crucial test of our prediction. We note that the model has three CP-violating phases, which are scanned as $-\pi \lesssim (\varphi, \phi_c, \phi_d) \lesssim \pi$ in our numerical analysis. It is possible to obtain the observed

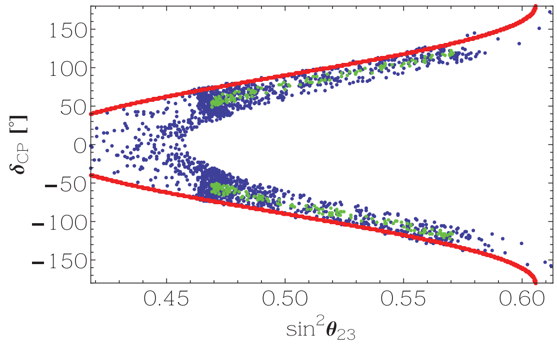

Fig. 1. The allowed region on the $\sin\theta_{23}$–δ_{CP} plane, where the blue and green dots correspond to the input of the $3\,\sigma$ and $1\,\sigma$ data in Table 2, respectively. The red curve represents the prediction of TM_2.

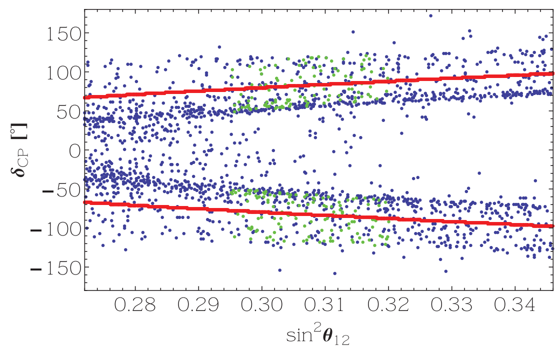

Fig. 2. The allowed region on the $\sin^2\theta_{12}$–δ_{CP} plane. The meaning of the colors is the same as in Fig. 1. The red curve represents the model without rotation to the neutrino mass matrix in the TBM basis.

values for the case of $\phi_c = \pm\pi$ and $\phi_d = 0$ in the neutrino mixing matrix. Then, we obtain the restricted predictions as $0.46 \lesssim \sin^2\theta_{23} \lesssim 0.48$ and $30° \lesssim |\delta_{CP}| \lesssim 60°$. In this case, the CP violation of leptons requires the source of the CP-violating phase φ in the charged lepton sector. On the other hand, it is also possible to obtain the observed values for the case of $\phi_d = 0$ and $\varphi = 0$ in the neutrino and charged lepton mixing matrices, respectively. In this case, the CP violation of leptons requires the source of the CP-violating phase ϕ_c in the neutrino sector.

Next, we show the prediction of δ_{CP} versus $\sin^2\theta_{12}$ in Fig. 2. The deviation from the trimaximal mixing of θ_{12} is due to the (1,3) family rotation of the charged lepton sector as seen in Eq. (22). The model without the additional rotation to the neutrino mass matrix in the TBM basis presented a clear correlation between $\sin^2\theta_{12}$ and δ_{CP} [27,28]. We also show its prediction by a red curve, which is obtained by taking the best-fit data in Table 2. Predicted points are scattered around the red curve. Our predicted region is broad for the $3\,\sigma$ data for the mixing angles. However, the $1\,\sigma$ data force the predicted region to be rather narrow. Then, $|\delta_{CP}| = 60$–$120°$ is predicted at the best fit of $\sin^2\theta_{12} = 0.307$, where the maximal CP violation $|\delta_{CP}| = 90°$ is still allowed.

On the other hand, we cannot find any correlation between δ_{CP} and $\sin^2\theta_{13}$ since both phases σ in the neutrino mass matrix and φ in the charged lepton mass matrix contribute to $\sin^2\theta_{13}$ as seen in Eq. (22). We do not present the result in a figure.

In order to understand the role of the key parameter α_η, we show how the three neutrino mixing angles and the CP-violating Dirac phase depend on α_η in Figs. 3–6. First, in Fig. 3, we show the prediction of $\sin\theta_{13}$ versus α_η where the $3\,\sigma$ data are taken as the input except for $\sin\theta_{13}$. The red

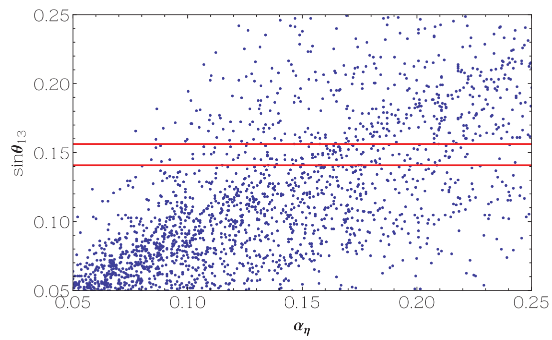

Fig. 3. The allowed region on the α_η–$\sin\theta_{13}$ plane, where the $3\,\sigma$ data are taken except for $\sin\theta_{13}$. The red lines represent the upper and lower bounds of the experimental data.

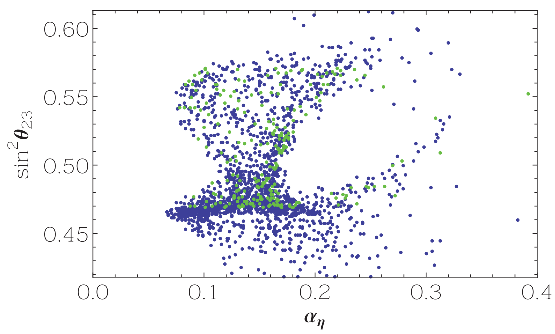

Fig. 4. The allowed region on the α_η–$\sin^2\theta_{23}$ plane. The meaning of colors is the same as in Fig. 1.

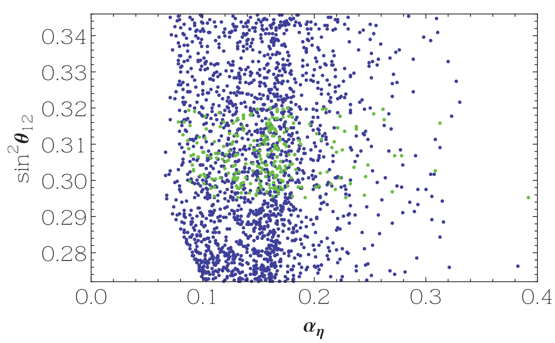

Fig. 5. The allowed region on the α_η–$\sin^2\theta_{12}$ plane. The meaning of colors is the same as in Fig. 1.

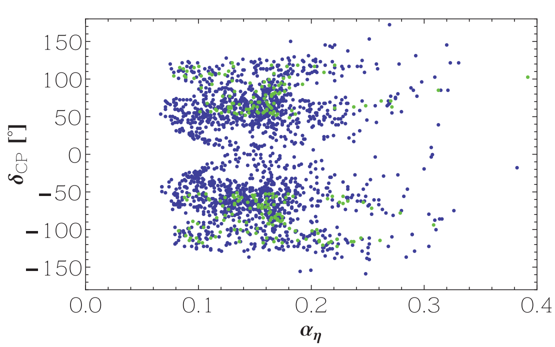

Fig. 6. The allowed region on the α_η–$\delta_{\rm CP}$ plane. The meaning of colors is the same as in Fig. 1.

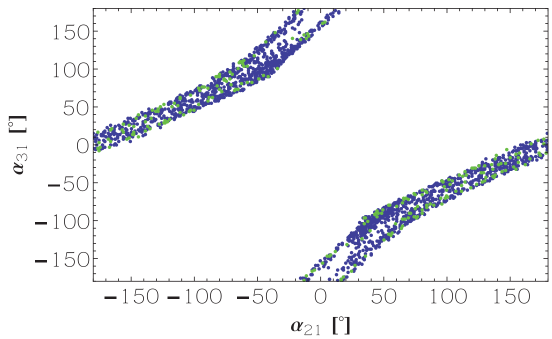

Fig. 7. The predicted Majorana phases on the α_{21}–α_{31} plane. The meaning of colors is the same as in Fig. 1.

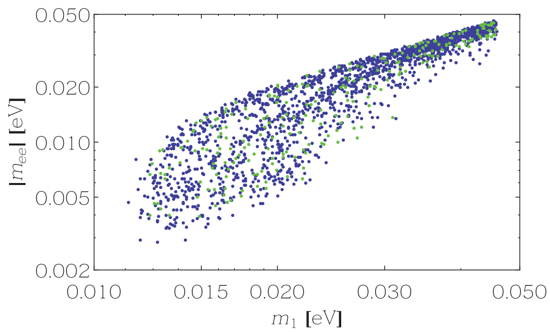

Fig. 8. The prediction of $|m_{ee}|$ versus m_1. The meaning of colors is the same as in Fig. 1.

lines denote the upper and lower bounds of the $3\,\sigma$ experimental data for $\sin\theta_{13}$. Note that $\sin\theta_{13}$ depends on α_η crucially as seen in Eq. (22). As shown in Fig. 3, the observed value $\sin\theta_{13}$ is not reproduced unless α_η is larger than 0.07.

The clear dependence between α_η and the predicted $\sin^2\theta_{23}$ can be seen in Fig. 4. In order to reproduce the maximal mixing of θ_{23}, α_η should be larger than 0.12. The highly probable prediction of $\sin^2\theta_{23}$ is near 0.47–0.5 for $0.1 \leq \alpha_\eta \leq 0.2$.

The deviation from the trimaximal mixing of $\sin^2\theta_{12}$ explicitly depends on α_η as seen in Eq. (22). We show the prediction of $\sin^2\theta_{12}$ versus α_η in Fig. 5. The predicted $\sin^2\theta_{12}$ is almost independent of α_η as long as $\alpha_\eta \geq 0.1$.

The α_η dependence on δ_{CP} gives the characteristic prediction as shown in Fig. 6. The CP conservation $\delta_{CP} = 0$ is excluded in the smaller region $\alpha_\eta \leq 0.12$ for the experimental data with $3\,\sigma$. By inputting the $1\,\sigma$ data in Table 2, we obtain the prediction of δ_{CP} as $\pm(50$–$120°)$, which is almost independent of α_η for $\alpha_\eta = 0.1$–0.2.

We show the prediction of the Majorana phases α_{21} and α_{31} in Fig. 7. While both Majorana phases are allowed in the full region of -180–$180°$, there is a clear correlation between both phases.

In Fig. 8, we present the predicted $|m_{ee}|$, the effective mass for the $0\nu\beta\beta$ decay, versus m_1, which is another key parameter in our model. The parameter m_1 should be larger than 12 meV in order to reproduce the observed mass-squared differences, and it is smaller than 46 meV due to the cosmological constraint on the sum of neutrino masses [26]. In the hierarchical case of neutrino masses $m_1 < m_2 \ll m_3$, the predicted value $|m_{ee}|$ is at most 10 meV but close to 45 meV for degenerate neutrino masses.

Next, we discuss the sum of three neutrino masses Σm_i because the cosmological observation gives us a upper bound for it. We show the predicted region of the Σm_i–$\sin^2\theta_{23}$ plane in Fig. 9.

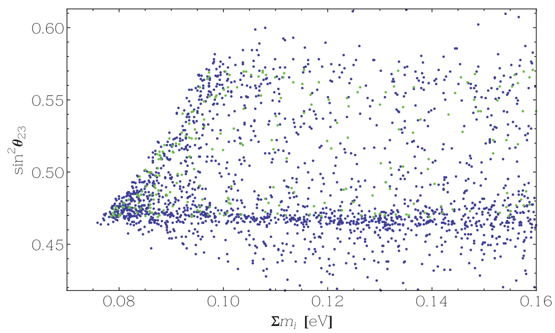

Fig. 9. The Σm_i dependence of the predicted $\sin^2\theta_{23}$. The meaning of colors is the same as in Fig. 1.

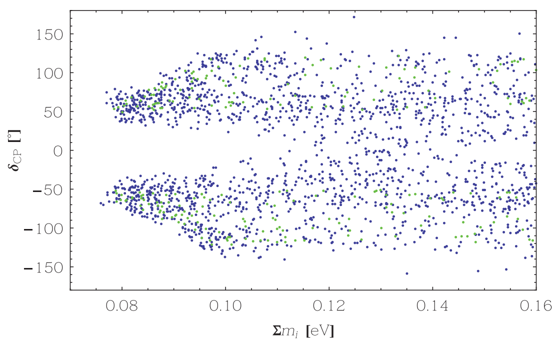

Fig. 10. The Σm_i dependence of the predicted δ_{CP}. The meaning of colors is the same as in Fig. 1.

The minimum of the sum of three neutrino masses Σm_i is 75 meV in our model. In order to get $\sin^2\theta_{23} \geq 0.5$, Σm_i should be larger than 85 meV. For the best fit of $\sin^2\theta_{23} = 0.538$, Σm_i is expected to be larger than 90 meV. We show the predicted region of the Σm_i–δ_{CP} plane in Fig. 10. The predicted $|\delta_{\mathrm{CP}}|$ is smaller than 90° if Σm_i is smaller than 85 meV. Thus, the cosmological observation for the sum of neutrino masses will be a crucial test of these predictions.

We have neglected the next-to-leading terms $ll\phi_S\phi_T h_u h_u$ and $ll\phi_T\eta h_u h_u$ in the neutrino mass matrix of Eq. (9) because $\alpha_\ell = 0.0316$ (0.010) is small compared with $\alpha_\eta \geq 0.1$. We have confirmed that those effects are small with our numerical calculation by inputting $1\,\sigma$ data. Indeed, the prediction of $\sin^2\theta_{23}$–δ_{CP} almost remains inside the red curve in Fig. 1.

It is also worthwhile commenting on the α_η distribution in our numerical results. In order to remove the predictions for $\alpha_\eta > 0.3$ smoothly, which is about ten times larger than $\alpha_\ell = 0.0316$, we have used the Gamma distribution for α_η given in Eq. (D3) of Appendix D. We have confirmed that our results are not changed even if we adopt another Gamma distribution presented in Eq. (D4) of Appendix D although the number density of dots gets lower. We have also used $\alpha_\ell = 0.010$, which corresponds to SM in our calculations. In this case, the number density of dots gets significantly lower, but the allowed region is almost unchanged. Moreover, we have found that the allowed region is also unchanged even if we use a flat distribution of α_η in the region $0 \leq \alpha_\eta \leq 0.3$. Thus, our results are robust for any distribution of α_η.

3.2. *Case of a* $1'$ *singlet* η

We show the numerical results for a $1'$ singlet η briefly because the correlations of the observables appear to be weak. We show the predicted δ_{CP} versus $\sin^2\theta_{23}$ in Fig.11. The region of $|\delta_{\mathrm{CP}}| \leq 50°$ is

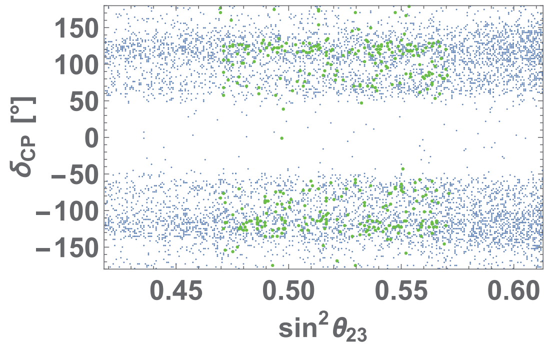

Fig. 11. The allowed region on the $\sin\theta_{23}$–δ_{CP} plane for $\eta(1')$. The meaning of colors is the same as in Fig. 1.

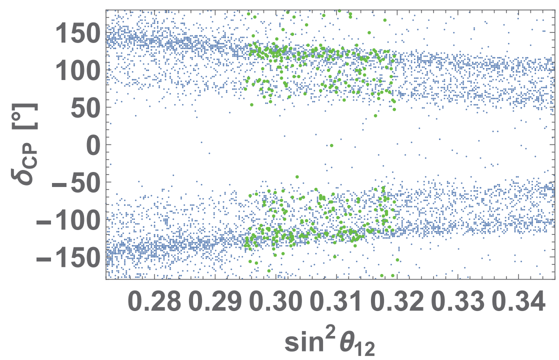

Fig. 12. The allowed region on the $\sin^2\theta_{12}$–δ_{CP} plane for $\eta(1')$. The meaning of colors is the same as in Fig. 1.

almost excluded while the regions near $\pm 180°$ are allowed. There is no correlation between $\sin^2\theta_{23}$ and δ_{CP}.

We also show the predicted δ_{CP} versus $\sin^2\theta_{12}$ in Fig. 12. The predicted $|\delta_{CP}|$ increases as $\sin^2\theta_{12}$ decreases from the trimaximal mixing $1/3$, but its correlation is rather weak.

Both results in Figs. 11 and 12 are due to mixing of the (1,2) and (2,3) families in the charged lepton sector. Thus, the model with the $1'$ singlet η is less attractive than that with the $1''$ singlet η in light of the NuFIT 3.2 data.

4. Summary

The flavor symmetry of leptons can be examined precisely in light of the new data and the upcoming experiments [29]. We study the A_4 model with minimal parameters by using the results of NuFIT 3.2. We introduce the A_4 singlet $1'$ or $1''$ flavon η, which couples to both the charged lepton and neutrino sectors in the next-to-leading order due to the relevant Z_3 charge for η. The model with the $1''$ ($1'$) flavon is consistent with the experimental data of $\Delta m^2_{\rm sol}$ only for NH of neutrino masses. The key parameter is α_η, which is derived from the VEV of the flavon η. The parameter α_η is distributed around $\alpha_\ell = 0.0316$ (0.010) in the Gamma distribution of the statistic. Our results are robust for different distributions of α_η.

In the case of the singlet $\eta(1'')$, α_η should be larger than 0.07 in order to reproduce the observed value of $\sin\theta_{13}$. The numerical prediction of δ_{CP} versus $\sin^2\theta_{23}$ is similar to the prediction of TM$_2$. However, our predicted region is inside the TM$_2$ boundary. The absolute value of the predicted δ_{CP} is 60–90° for the maximal mixing $\theta_{23} = \pi/4$. For the best fit of $\sin^2\theta_{23} = 0.538$, $|\delta_{CP}|$ is in the region of 90–110°. The predicted $\sin^2\theta_{12}$ is also allowed around the best fit of NuFIT 3.2 while staying near the maximal mixing of θ_{23}. Inputting the data with the $1\,\sigma$ error-bar, we obtain a clear prediction of the CP-violating Dirac phase of $|\delta_{\rm CP}| = 50$–120°. The lightest neutrino mass m_1 is expected to be 12–46 meV, which leads to $|m_{ee}| < 45$ meV. In order to get the best fit of $\sin^2\theta_{23} = 0.538$, the sum of the three neutrino masses is expected to be larger than 90 meV. The cosmological observation for the sum of the neutrino masses will also provide a crucial test of these predictions.

The model with $\eta(1')$ is not attractive in light of the NuFIT 3.2 result because the input data given in Table 2 do not give a severe constraint for the predicted region of $\delta_{\rm CP}$.

We expect a precise measurement of the CP-violating phase to test the model in the future.

Acknowledgements

This work is supported by Japan Society for the Promotion of Science (JSPS) Grants-in-Aid for Scientific Research 16J05332 (Y.S.) and 15K05045, 16H00862 (M.T.). S.K.K. was supported by the National Research Foundation of Korea (NRF) grants (2009-0083526, 2017K1A3A7A09016430, 2017R1A2B4006338).

Funding

Open Access funding: SCOAP[3].

Appendix A. Lepton mixing matrix

Supposing neutrinos to be Majorana particles, the PMNS matrix $U_{\rm PMNS}$ [24,25] is parametrized in terms of the three mixing angles θ_{ij} $(i,j = 1,2,3;\ i < j)$, one CP-violating Dirac phase $\delta_{\rm CP}$, and two Majorana phases α_{21}, α_{31} as follows:

$$U_{\rm PMNS} = \begin{pmatrix} c_{12}c_{13} & s_{12}c_{13} & s_{13}e^{-i\delta_{\rm CP}} \\ -s_{12}c_{23} - c_{12}s_{23}s_{13}e^{i\delta_{\rm CP}} & c_{12}c_{23} - s_{12}s_{23}s_{13}e^{i\delta_{\rm CP}} & s_{23}c_{13} \\ s_{12}s_{23} - c_{12}c_{23}s_{13}e^{i\delta_{\rm CP}} & -c_{12}s_{23} - s_{12}c_{23}s_{13}e^{i\delta_{\rm CP}} & c_{23}c_{13} \end{pmatrix} \begin{pmatrix} 1 & 0 & 0 \\ 0 & e^{i\frac{\alpha_{21}}{2}} & 0 \\ 0 & 0 & e^{i\frac{\alpha_{31}}{2}} \end{pmatrix}, \tag{A1}$$

where c_{ij} and s_{ij} denote $\cos\theta_{ij}$ and $\sin\theta_{ij}$, respectively.

The rephasing invariant CP-violating measure, the Jarlskog invariant [30], is defined by the PMNS matrix elements $U_{\alpha i}$. It is written in terms of the mixing angles and the CP-violating phase as:

$$J_{\rm CP} = {\rm Im}\left[U_{e1}U_{\mu 2}U_{e2}^*U_{\mu 1}^*\right] = s_{23}c_{23}s_{12}c_{12}s_{13}c_{13}^2\sin\delta_{\rm CP}, \tag{A2}$$

where $U_{\alpha i}$ denotes each component of the PMNS matrix.

There are also other invariants I_1 and I_2 associated with Majorana phases [31–35]:

$$I_1 = {\rm Im}\left[U_{e1}^*U_{e2}\right] = c_{12}c_{12}c_{13}^2\sin\left(\frac{\alpha_{21}}{2}\right), \quad I_2 = {\rm Im}\left[U_{e1}^*U_{e3}\right] = c_{12}s_{13}c_{13}\sin\left(\frac{\alpha_{31}}{2} - \delta_{\rm CP}\right). \tag{A3}$$

We calculate $\delta_{\rm CP}$, α_{21}, and α_{31} with these relations.

Appendix B. Multiplication rule of the A_4 group

We use the multiplication rule of the A_4 triplet as follows:

$$\begin{pmatrix} a_1 \\ a_2 \\ a_3 \end{pmatrix}_{\mathbf{3}} \otimes \begin{pmatrix} b_1 \\ b_2 \\ b_3 \end{pmatrix}_{\mathbf{3}} = (a_1b_1 + a_2b_3 + a_3b_2)_{\mathbf{1}} \oplus (a_3b_3 + a_1b_2 + a_2b_1)_{\mathbf{1'}}$$

$$\oplus\,(a_2b_2+a_1b_3+a_3b_1)_{\mathbf{1}''}$$
$$\oplus\,\frac{1}{3}\begin{pmatrix}2a_1b_1-a_2b_3-a_3b_2\\2a_3b_3-a_1b_2-a_2b_1\\2a_2b_2-a_1b_3-a_3b_1\end{pmatrix}_{\mathbf{3}}\oplus\,\frac{1}{2}\begin{pmatrix}a_2b_3-a_3b_2\\a_1b_2-a_2b_1\\a_3b_1-a_1b_3\end{pmatrix}_{\mathbf{3}},$$
$$\mathbf{1}\otimes\mathbf{1}=\mathbf{1},\qquad \mathbf{1}'\otimes\mathbf{1}'=\mathbf{1}'',\qquad \mathbf{1}''\otimes\mathbf{1}''=\mathbf{1}',\qquad \mathbf{1}'\otimes\mathbf{1}''=\mathbf{1}\,. \tag{B1}$$

More details are shown in Refs. [15,16].

Appendix C. Charged lepton and neutrino mass matrices

The left-handed mixing matrix of the charged lepton is derived from the diagonalization of $U_\ell M_\ell M_\ell^\dagger U_\ell^\dagger$ in Eq. (5). The diagonalizing matrix $U_l^\dagger$ for the charged lepton is given as follows:

$$U_\ell^\dagger\simeq\begin{pmatrix}1 & -\frac{y'_\mu}{y_\mu}\frac{y'_\tau}{y_\tau}\alpha_\eta^2 & \frac{y'_\tau}{y_\tau}\alpha_\eta\\ (\frac{y'_\mu}{y_\mu}\frac{y'_\tau}{y_\tau})^*\alpha_\eta^2 & 1 & \frac{y_\mu y'^*_\mu}{|y_\tau|^2}\alpha_\eta\lambda^4\\ -(\frac{y'_\tau}{y_\tau})^*\alpha_\eta & \frac{y'_\mu}{y_\mu}|\frac{y'_\tau}{y_\tau}|^2\alpha_\eta^3 & 1\end{pmatrix}\quad \text{for } \eta\ (1''),$$
$$U_\ell^\dagger\simeq\begin{pmatrix}1 & \frac{y'_\mu}{y_\mu}\alpha_\eta & \frac{y'_\tau}{y_\tau}\frac{y'_\mu}{y_\tau}(\frac{y_\mu}{y_\tau})^*\alpha_\eta^2\lambda^4\\ -(\frac{y'_\mu}{y_\mu})^*\alpha_\eta & 1 & \frac{y'_\tau}{y_\tau}\alpha_\eta\\ (\frac{y'_\mu}{y_\mu}\frac{y'_\tau}{y_\tau})^*\alpha_\eta^2 & -(\frac{y'_\tau}{y_\tau})^*\alpha_\eta & 1\end{pmatrix}\quad \text{for } \eta\ (1'). \tag{C1}$$

The mass eigenvalues of the charged leptons are given in a good approximation:

$$m_e=|y_e|\alpha_\ell\lambda^4 v_d,\quad m_\mu=|y_\mu|\alpha_\ell\lambda^2 v_d,\quad m_\tau=|y_\tau|\alpha_\ell v_d, \tag{C2}$$

where the Yukawa couplings are of order one.

Next, we consider the neutrino mass matrix in the TBM basis. $\hat{M}_\nu\hat{M}_\nu^\dagger$ is written as follows:

$$\hat{M}_\nu\hat{M}_\nu^\dagger=\begin{pmatrix}(1,1) & 0 & (1,3)\\ 0 & |ce^{i\phi_c}+de^{i\phi_d}|^2 & 0\\ (1,3)^* & 0 & (3,3)\end{pmatrix}, \tag{C3}$$

where

$$\begin{aligned}(1,1)&=a^2+c^2+d^2+2ac\cos\phi_c-cd\cos(\phi_c-\phi_d)-ad\cos\phi_d,\\ (3,3)&=a^2+c^2+d^2-2ac\cos\phi_c-cd\cos(\phi_c-\phi_d)+ad\cos\phi_d,\\ (1,3)&=\mp\sqrt{3}\,[ad\cos\phi_d+icd\sin(\phi_c-\phi_d)].\end{aligned} \tag{C4}$$

Here, the upper (lower) sign in front of the (1,3) component corresponds to the assignment of $1''$ and $1'$ for η, respectively. We obtain the neutrino mass eigenvalues for NH as follows:

$$\begin{aligned}m_1^2=&\,a^2+c^2+d^2-cd\cos(\phi_c-\phi_d)\\ &-\sqrt{3c^2d^2\sin^2(\phi_c-\phi_d)+4a^2(c^2\cos^2\phi_c+d^2\cos^2\phi_d-cd\cos\phi_c\cos\phi_d)},\end{aligned}$$

$$
\begin{aligned}
m_3^2 &= a^2 + c^2 + d^2 - cd\cos(\phi_c - \phi_d) \\
&\quad + \sqrt{3c^2d^2\sin^2(\phi_c - \phi_d) + 4a^2(c^2\cos^2\phi_c + d^2\cos^2\phi_d - cd\cos\phi_c\cos\phi_d)}, \\
m_2^2 &= c^2 + d^2 + 2cd\cos(\phi_c - \phi_d).
\end{aligned} \tag{C5}
$$

$\hat{M}_\nu \hat{M}_\nu^\dagger$ is diagonalized by the (1,3) family rotation as:

$$
U_\nu\ (\hat{M}_\nu \hat{M}_\nu^\dagger)\ U_\nu^\dagger = \begin{pmatrix} m_1^2 & 0 & 0 \\ 0 & m_2^2 & 0 \\ 0 & 0 & m_3^2 \end{pmatrix}, \tag{C6}
$$

where

$$
U_\nu^\dagger = \begin{pmatrix} \cos\theta & 0 & \sin\theta e^{-i\sigma} \\ 0 & 1 & 0 \\ -\sin\theta e^{i\sigma} & 0 & \cos\theta \end{pmatrix}. \tag{C7}
$$

θ and σ are given in terms of parameters in the neutrino mass matrix:

$$
\tan 2\theta = \sqrt{3}\,\frac{d\sqrt{a^2\cos^2\phi_d + c^2\sin^2(\phi_c - \phi_d)}}{a(d\cos\phi_d - 2c\cos\phi_c)}, \qquad \tan\sigma = -\frac{c\sin(\phi_c - \phi_d)}{a\cos\phi_d}. \tag{C8}
$$

The parameters a, c, and d are written in terms of m_1 and α_η. As seen in Eq. (10) , the parameter d is related to c as

$$
\frac{d}{c} = \left|\frac{y_7'}{y_\xi}\right| \alpha_\eta \equiv \alpha_\eta^\nu, \tag{C9}
$$

where y_7' and y_ξ are order-one coefficients. On the other hand, a and c are given in terms of m_1, α_η^ν, $\Delta m_{31}^2 \equiv m_3^2 - m_1^2$, and $\Delta m_{21}^2 \equiv m_3^2 - m_1^2$ since we have the following relations in Eq. (C5):

$$
\begin{aligned}
\frac{1}{4}(\Delta m_{31}^2)^2 &= 3c^2d^2\sin^2(\phi_c - \phi_d) + 4a^2(c^2\cos^2\phi_c + d^2\cos^2\phi_d - cd\cos\phi_c\cos\phi_d), \\
\Delta m_{21}^2 &= c^2 + d^2 + 2cd\cos(\phi_c - \phi_d) - m_1^2.
\end{aligned} \tag{C10}
$$

Then, putting $\Delta m_{\rm atm}^2 = \Delta m_{31}^2$ and $\Delta m_{\rm sol}^2 = \Delta m_{21}^2$,

$$
c^2 = \frac{\Delta m_{\rm sol}^2 + m_1^2}{1 + (\alpha_\eta^\nu)^2 + 2\alpha_\eta^\nu\cos(\phi_c - \phi_d)}, \quad a^2 = \frac{1}{16c^2}\,\frac{\Delta m_{\rm atm}^2 - 12c^4(\alpha_\eta^\nu)^2\sin^2(\phi_c - \phi_d)}{\cos^2\phi_c + (\alpha_\eta^\nu)^2\cos^2\phi_d - \alpha_\eta^\nu\cos\phi_c\cos\phi_d}, \tag{C11}
$$

where m_1 and α_η^ν are free parameters as well as ϕ_c and ϕ_d.

We comment on the case of IH of neutrino masses. In this case, the neutrino mass eigenvalues are given as

$$
\begin{aligned}
m_1^2 &= a^2 + c^2 + d^2 - cd\cos(\phi_c - \phi_d) \\
&\quad + \sqrt{3c^2d^2\sin^2(\phi_c - \phi_d) + 4a^2(c^2\cos^2\phi_c + d^2\cos^2\phi_d - cd\cos\phi_c\cos\phi_d)},
\end{aligned}
$$

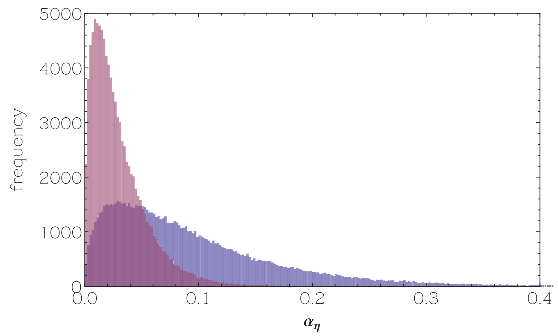

Fig. D1. α_η distribution for $\alpha_\ell = 0.0316$ (blue) and $\alpha_\ell = 0.010$ (red) in Eq. (D3) ($\alpha = 3/2, \beta = 2, \gamma = 1, \mu = 0$).

$$m_3^2 = a^2 + c^2 + d^2 - cd\cos(\phi_c - \phi_d) - \sqrt{3c^2d^2\sin^2(\phi_c-\phi_d) + 4a^2(c^2\cos^2\phi_c + d^2\cos^2\phi_d - cd\cos\phi_c\cos\phi_d)},$$
$$m_2^2 = c^2 + d^2 + 2cd\cos(\phi_c - \phi_d), \tag{C12}$$

where m_1^2 and m_3^2 are exchanged with each other in Eq. (C5). Then, $\Delta m^2_{\rm sol}$ is given as

$$\Delta m^2_{\rm sol} = m_2^2 - m_1^2 = 3cd\cos(\phi_c-\phi_d) - a^2 - \sqrt{3c^2d^2\sin^2(\phi_c-\phi_d) + 4a^2(c^2\cos^2\phi_c + d^2\cos^2\phi_d - cd\cos\phi_c\cos\phi_d)}. \tag{C13}$$

It is impossible to reproduce the observed value of $\Delta m^2_{\rm sol}$ since $a \sim c$ and $c \gg d$ in our model as seen in Eq. (10). Indeed, d/c is expected to be 0.1–0.2 in our numerical analysis.

Appendix D. Distribution of α_η

The magnitude of the parameter α_ℓ is determined by the tau-lepton mass as seen in Eq. (24). The key parameter α_η is related to α_ℓ through the vacuum structure as discussed in Eq. (4):

$$\alpha_\eta = \frac{\lambda_1}{\lambda_2}\sqrt{\frac{g_4}{3g_3}}\,\alpha_\ell. \tag{D1}$$

The coefficients $\lambda_{1(2)}$ and $g_{3(4)}$ are of order one. Then, the factor in front of α_ℓ in Eq. (D1) could be $\mathcal{O}(10)$. We scan α_η by using Eq. (D1) after fixing α_ℓ in the statistical approach. For this purpose, we use the Gamma distribution that is available to find the distribution of the order-one parameter:

$$f = (x-\mu)^{(\alpha\gamma-1)} e^{\left(\frac{x-\mu}{\beta}\right)^\gamma}. \tag{D2}$$

Taking $\gamma = 1$ with $\alpha = 3/2$, $\mu = 0$, and $\beta = 2$, we obtain

$$f = \sqrt{x}\, e^{-\frac{1}{2}x}, \tag{D3}$$

which is equivalent to the χ^2 distribution. When we take $\gamma = 2$ with $\alpha = 1$, $\mu = 0$, and $\beta = \sqrt{2}$, we obtain

$$f = x\, e^{-\frac{1}{2}x^2}, \tag{D4}$$

which damps like a Gaussian distribution at large x.

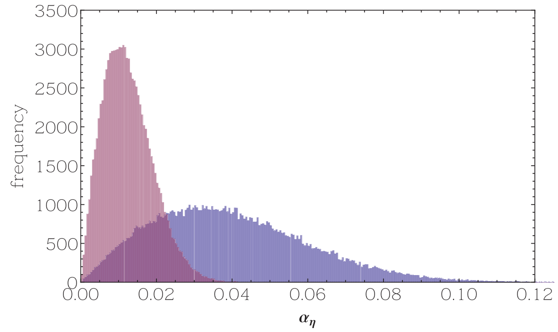

Fig. D2. α_η distribution for $\alpha_\ell = 0.0316$ (blue) and $\alpha_\ell = 0.010$ (red) in Eq. (D4) ($\alpha = 1, \beta = \sqrt{2}$, $\gamma = 2, \mu = 0$).

It is easy to check that f is maximal at $x = 1$ and $f = 0$ at $x = 0$ for both types of Gamma distribution. We obtain the distribution of α_η by multiplying α_ℓ by f, which is used in our numerical calculations. We show the distribution of α_η in Figs. D1 and D2 for $\alpha_\ell = 0.0316$ (MSSM $\tan\beta = 3$) and $\alpha_\ell = 0.010$ (SM) in the case of the distributions of Eqs. (D3) and (D4), respectively.

References

[1] K. Abe et al. [T2K Collaboration], Phys. Rev. D **96**, 092006 (2017) [arXiv:1707.01048 [hep-ex]] [Search INSPIRE].
[2] *T2K report* (2017) (available at: http://t2k-experiment.org/2017/08/t2k-2017-cpv/).
[3] P. Adamson et al. [NOvA Collaboration], Phys. Rev. Lett. **118**, 231801 (2017) [arXiv:1703.03328 [hep-ex]] [Search INSPIRE].
[4] A. Radovic, "Latest oscillation results from NOvA." Joint Experimental-Theoretical Physics Seminar, Fermilab, USA, January 12, 2018.
[5] *NuFIT 3.2* (2018) (available at: www.nu-fit.org).
[6] F. P. An et al. [DAYA-BAY Collaboration], Phys. Rev. Lett. **108**, 171803 (2012) [arXiv:1203.1669 [hep-ex]] [Search INSPIRE].
[7] J. K. Ahn et al. [RENO Collaboration], Phys. Rev. Lett. **108**, 191802 (2012) [arXiv:1204.0626 [hep-ex]] [Search INSPIRE].
[8] P. F. Harrison, D. H. Perkins, and W. G. Scott, Phys. Lett. B **530**, 167 (2002) [arXiv:hep-ph/0202074] [Search INSPIRE].
[9] P. F. Harrison and W. G. Scott, Phys. Lett. B **535**, 163 (2002) [arXiv:hep-ph/0203209] [Search INSPIRE].
[10] E. Ma and G. Rajasekaran, Phys. Rev. D **64**, 113012 (2001) [arXiv:hep-ph/0106291] [Search INSPIRE].
[11] K. S. Babu, E. Ma, and J. W. F. Valle, Phys. Lett. B **552**, 207 (2003) [arXiv:hep-ph/0206292] [Search INSPIRE].
[12] G. Altarelli and F. Feruglio, Nucl. Phys. B **720**, 64 (2005) [arXiv:hep-ph/0504165] [Search INSPIRE].
[13] G. Altarelli and F. Feruglio, Nucl. Phys. B **741**, 215 (2006) [arXiv:hep-ph/0512103] [Search INSPIRE].
[14] G. Altarelli and F. Feruglio, Rev. Mod. Phys. **82**, 2701 (2010) [arXiv:1002.0211 [hep-ph]] [Search INSPIRE].
[15] H. Ishimori, T. Kobayashi, H. Ohki, Y. Shimizu, H. Okada, and M. Tanimoto, Prog. Theor. Phys. Suppl. **183**, 1 (2010) [arXiv:1003.3552 [hep-th]] [Search INSPIRE].
[16] H. Ishimori, T. Kobayashi, H. Ohki, H. Okada, Y. Shimizu, and M. Tanimoto, *An Introduction to Non-Abelian Discrete Symmetries for Particle Physicists* (Springer, Berlin, 2012), Lecture Notes in Physics Vol. 858, p. 1.
[17] S. F. King, A. Merle, S. Morisi, Y. Shimizu, and M. Tanimoto, New J. Phys. **16**, 045018 (2014) [arXiv:1402.4271 [hep-ph]] [Search INSPIRE].
[18] Y. Shimizu, M. Tanimoto, and A. Watanabe, Prog. Theor. Phys. **126**, 81 (2011) [arXiv:1105.2929 [hep-ph]] [Search INSPIRE].

[19] W. Grimus and L. Lavoura, J. High Energy Phys. **0809**, 106 (2008) [arXiv:0809.0226 [hep-ph]] [Search INSPIRE].
[20] C. H. Albright, A. Dueck, and W. Rodejohann, Eur. Phys. J. C **70**, 1099 (2010) [arXiv:1004.2798 [hep-ph]] [Search INSPIRE].
[21] W. Rodejohann and H. Zhang, Phys. Rev. D **86**, 093008 (2012) [arXiv:1207.1225 [hep-ph]] [Search INSPIRE].
[22] C. D. Froggatt and H. B. Nielsen, Nucl. Phys. B **147**, 277 (1979).
[23] G. Altarelli, F. Feruglio, and C. Hagedorn, J. High Energy Phys. **0803**, 052 (2008) [arXiv:0802.0090 [hep-ph]] [Search INSPIRE].
[24] Z. Maki, M. Nakagawa, and S. Sakata, Prog. Theor. Phys. **28**, 870 (1962).
[25] B. Pontecorvo, Sov. Phys. JETP **26**, 984 (1968) [Zh. Eksp. Teor. Fiz. **53**, 1717 (1967)].
[26] E. Giusarma, M. Gerbino, O. Mena, S. Vagnozzi, S. Ho, and K. Freese, Phys. Rev. D **94**, 083522 (2016) [arXiv:1605.04320 [astro-ph.CO]] [Search INSPIRE].
[27] Y. Shimizu, M. Tanimoto, and K. Yamamoto, Mod. Phys. Lett. A **30**, 1550002 (2015) [arXiv:1405.1521 [hep-ph]] [Search INSPIRE].
[28] S. K. Kang and M. Tanimoto, Phys. Rev. D **91**, 073010 (2015) [arXiv:1501.07428 [hep-ph]] [Search INSPIRE].
[29] S. T. Petcov and A. V. Titov, Phys. Rev. D **97**, 115045 (2018) [arXiv:1804.00182 [hep-ph]] [Search INSPIRE].
[30] C. Jarlskog, Phys. Rev. Lett. **55**, 1039 (1985).
[31] S. M. Bilenky, S. Pascoli, and S. T. Petcov, Phys. Rev. D **64**, 053010 (2001) [arXiv:hep-ph/0102265] [Search INSPIRE].
[32] J. F. Nieves and P. B. Pal, Phys. Rev. D **36**, 315 (1987).
[33] J. F. Nieves and P. B. Pal, Phys. Rev. D **64**, 076005 (2001) [arXiv:hep-ph/0105305] [Search INSPIRE].
[34] J. A. Aguilar-Saavedra and G. C. Branco, Phys. Rev. D **62**, 096009 (2000) [arXiv:hep-ph/0007025] [Search INSPIRE].
[35] I. Girardi, S. T. Petcov, and A. V. Titov, Nucl. Phys. B **911**, 754 (2016) [arXiv:1605.04172 [hep-ph]] [Search INSPIRE].